

**CALCAREOUS NANNOPLANKTON ASSEMBLAGES ACROSS THE
PLIOCENE-PLEISTOCENE TRANSITION IN THE SOUTHWESTERN
INDIAN OCEAN, IODP SITE U1475**

An Undergraduate Research Scholars Thesis

by

C. LAYNE FARR and ZOE P. CARES

Submitted to the Undergraduate Research Scholars program at
Texas A&M University
in partial fulfillment of the requirements for the designation as an

UNDERGRADUATE RESEARCH SCHOLAR

Approved by Research Advisor:

Dr. Leah J. LeVay

May 2018

Major: B.S. Geology
B.S. Environmental Geosciences

TABLE OF CONTENTS

	Page
ABSTRACT	1
ACKNOWLEDGMENTS	2
NOMENCLATURE	3
CHAPTERS	
I. INTRODUCTION.....	4
II. METHODOLOGY	8
Sample Preparation.....	8
<i>Reticulofenestra</i> Classification Scheme	8
Analytical Methods	9
III. RESULTS.....	12
Richness and Diversity	12
Full Assemblage Details	13
Full Assemblage Details Excluding the <i>Reticulofenestra</i> $\leq 5 \mu\text{m}$ Signal	14
Individual Species and Genera Details Excluding the <i>Reticulofenestra</i> $\leq 5 \mu\text{m}$ Signal	15
IV. DISCUSSION.....	19
Nannoplankton as Environmental Indicators.....	19
Warm-Water Indicators	19
Cold-Water Indicators	20
<i>Reticulofenestra</i> $\leq 5 \mu\text{m}$, <i>R. pseudoumbilicus</i> $> 5 \mu\text{m}$, and <i>R. antarcticus</i> $> 5 \mu\text{m}$	20
Environmental Change Across the Pliocene-Pleistocene Transition	20
V. CONCLUSION.....	23
REFERENCES	24
APPENDIX.....	28

ABSTRACT

Calcareous Nannoplankton Assemblages across the Pliocene-Pleistocene Transition in the Southwestern Indian Ocean, IODP Site U1475

C. Layne Farr
Department of Geology and Geophysics
Texas A&M University

Zoe P. Cares
Department of Environmental Programs in Geosciences
Texas A&M University

Research Advisor: Dr. Leah J. LeVay
International Ocean Discovery Program
Texas A&M University

International Ocean Discovery Program (IODP) Expedition 361 cored six sites along the greater Agulhas Current system. An objective of this expedition was to determine the dynamics of the Indian-Atlantic Ocean Gateway circulation during Pliocene-Pleistocene climate changes in association with changing wind fields and migrating ocean fronts. The Indian-Atlantic Ocean Gateway contains a pronounced oceanic frontal system, the position of which has the potential to influence global climate on millennial scales. Owing to the physical differences between the frontal zones, this region has complex biogeochemistry, changes in phytoplankton distribution, and variations in primary productivity. Site U1475 was cored on the Agulhas Plateau in the Southwestern Indian Ocean and recovered a complete sequence of calcareous ooze spanning the last ~7 Ma. The calcareous nannoplankton assemblage shows an increase of taxa associated with cooler water across the Pliocene-Pleistocene Transition (PPT) interval suggesting that a long-term change in sea surface temperature and nutrient availability took place across the PPT, potentially linked to the northward migration of the Subtropical Front.

ACKNOWLEDGEMENTS

This research used samples provided by the International Ocean Discovery Program. We would like to thank the IODP Expedition 361 science party, technicians, and crew for making this research project possible.

We would like to give special thanks to International Ocean Discovery Program expedition project manager and staff scientist Dr. Leah J. LeVay for her active role as our undergraduate research advisor. Her unceasing encouragement, mentorship, and assistance in this research project allowed for our success as Undergraduate Research Scholars. Without her positivity, care, and openness to communication, our time as researchers would not have been so enjoyable. Leah has truly provided us with a spectacular research experience.

We would like to thank the Texas A&M College of Geosciences for funding during our travel and lodging at various scientific conferences. These conferences proved to be unforgettable experiences and opportunities to present our scientific research in its various stages of development.

We would like to thank the Undergraduate Research Scholars Program for helping us cultivate our skills as researchers and academics through the requirements as an Undergraduate Research Scholar. This program has proven to be a fantastic capstone for us, concluding our efforts on this undergraduate research project.

Finally, we would like to thank our beloved friends and family for their continuous comfort and support.

NOMENCLATURE

μm	Micron
FOV	Field of view
H	Shannon diversity index value
IAOG	Indian-Atlantic Ocean Gateway
IODP	International Ocean Discovery Program
Kyr	Thousand years
m	Meters
Ma	Million years ago
mbsf	Meters below seafloor
nmi	Nautical miles
PPT	Pliocene-Pleistocene transition

CHAPTER 1

INTRODUCTION

Ocean circulation through the Indian-Atlantic Ocean Gateway (IAOG) is interconnected to high-latitude climate forcing on geologic timescales. The IAOG (Figure 1) contains a pronounced oceanic frontal system, the position of which has the potential to influence global climate on millennial scales. One of the key components of the Indian-Atlantic gateway is the

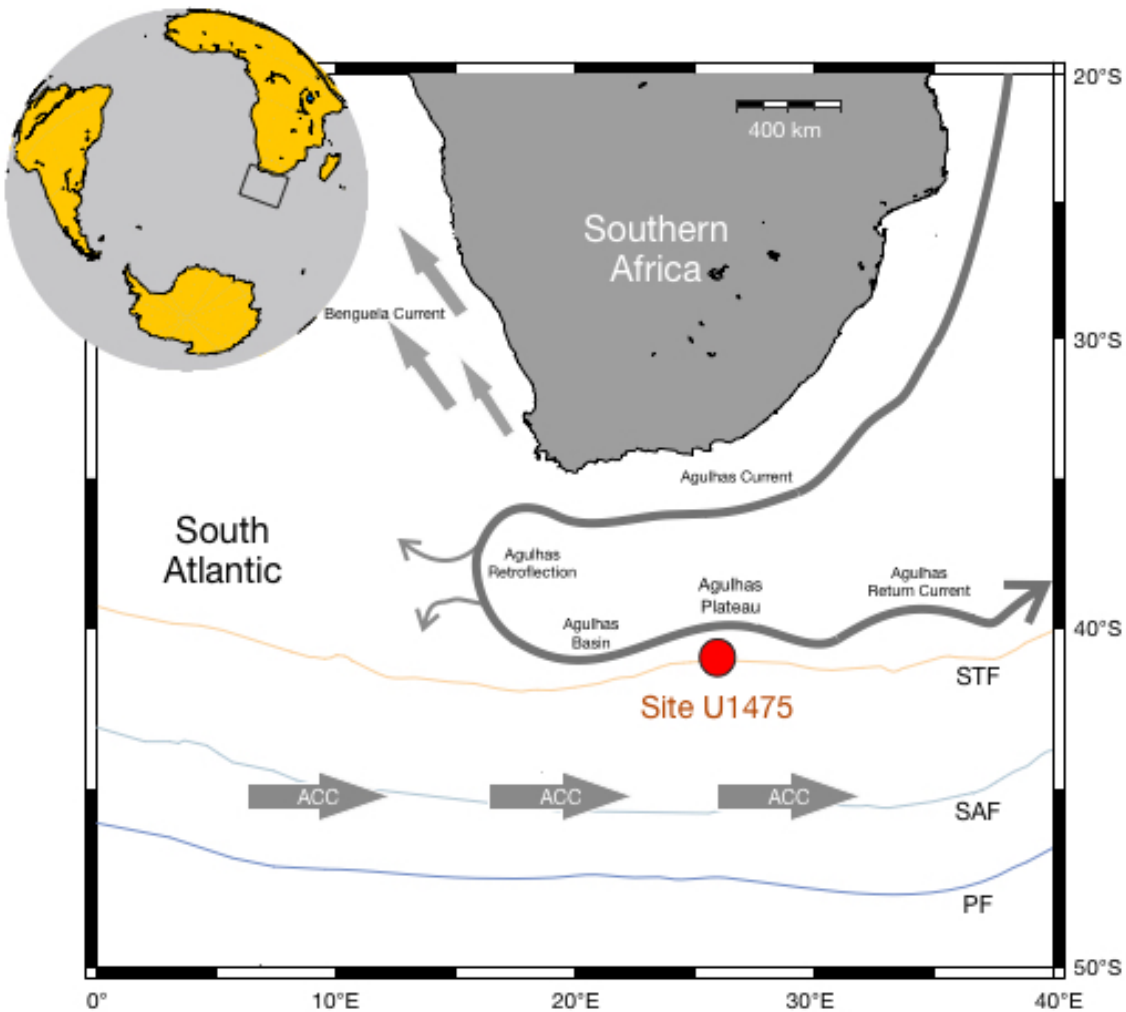


Figure 1. Adapted from Romero et al., 2015. Present location of the Agulhas Current and Southern Ocean Fronts in the Southern Ocean. Full lines represent the position of the Polar Front (PF), Sub-Antarctic Front (SAF), Sub-Tropical Front (STF), and the Agulhas Current. The red dot shows the location of Site U1475 on the Agulhas Plateau. The Antarctic Circumpolar Current (ACC) is also represented with gray arrows.

Agulhas Current, a large western boundary current that runs along the southeastern coast of Africa. Fluctuations in global climate and Antarctic glaciation have resulted in the latitudinal migration of the Agulhas Current and Southern Ocean Fronts (McKay et al., 2012; Romero et al., 2015; Hall et al., 2017). It has been suggested that northward shifts of these frontal zones led to intensified Northern Hemisphere glaciation (Bard and Rickaby, 2009).

The late Pliocene (~3 Ma) was characterized by atmospheric $p\text{CO}_2$ concentrations ~35% higher than modern pre-industrial levels (Raymo, 1996), ocean temperatures ~3° C warmer than modern oceans (Cronin, 1991), and major-deglaciation of the East Antarctic ice sheet (Barrett, 1992). From ~4 - 1.5 Ma, subtle changes in the atmospheric greenhouse gas composition, basin geometry, or land-surface conditions allowed the earth to cool gradually (Ravelo, 2004). Global cooling during the Pliocene-Pleistocene Transition (PPT) is postulated to be a result of a high-latitude response to decreasing atmospheric $p\text{CO}_2$ levels (Sosdian et al., 2009) and was marked by major Northern Hemisphere glaciation at ~2.7 Ma and Antarctic ice sheet expansion.

Maximal $p\text{CO}_2$ in the Pliocene atmosphere gradually declined from ~410 μatm to maximal Pleistocene values of 300 μatm at 2.0 Ma (Bartoli et al., 2011). Late Pliocene cooling has been associated with increases in wind-driven upwelling, creating long-term sinks for atmospheric CO_2 on the eastern boundaries of major ocean basins (Marlow, 2000). The expansion of Antarctic ice sheets may have altered Southern Ocean Circulation and restricted the Agulhas Current from flowing into the Atlantic (McKay et al., 2012).

Latitudinal migration of the Southern Ocean Fronts have occurred in the Quaternary as is evident by diatom production increases. Increased availability of nutrients in the surface waters during the Late Pleistocene glacial cycles, allowed for increased diatom productivity (Romero et al., 2015). The northward migration of the Agulhas Return Current and Southern Ocean Fronts

during Late Pleistocene glacial cycles caused shifts in primary production and biological pump efficiency, driving the diatom assemblage variations along the southern Agulhas Plateau.

Another phytoplankton group that is sensitive to changes in temperature and nutrient availability is coccolithophores. A deep-sea record millions of years old is preserved by the calcium carbonate shell of coccolithophores. These extant unicellular marine plants are included as part of the fossilized group termed calcareous nannoplankton (Weier, 1999).

Coccolithophorids contribute to oceanic productivity across the globe and through large blooms that are able to grow in polar regions with poor levels of nutrients. Variations in nannoplankton assemblages are used to identify changes in primary productivity and sea surface temperatures (e.g., Marino et al., 2009). In turn, these fossils allow for insight into global climate variability and have been used for such in sites all around the world (Marino et al., 2011). Their role as a proxy is appropriate, as slight environmental changes are shown directly in their rates of productivity (Marlow et al., 2000).

We hypothesize that cooling across the PPT would cause an observable change in the calcareous nannoplankton assemblage, which could be related to the northward migration of the Southern Ocean fronts. This project will extend the record of frontal migration history in the Indian-Atlantic Ocean Gateway back to the late Pliocene. In addition, this record will aid in understanding the role of the IAOG in global climate and oceanographic changes and allow us to test if Antarctic ice sheet expansion influenced this region. We will achieve this by analyzing the abundance and diversity of the calcareous nannoplankton assemblage and using the paleoecology of nannoplankton to reconstruct relative surface water temperature changes and productivity changes.

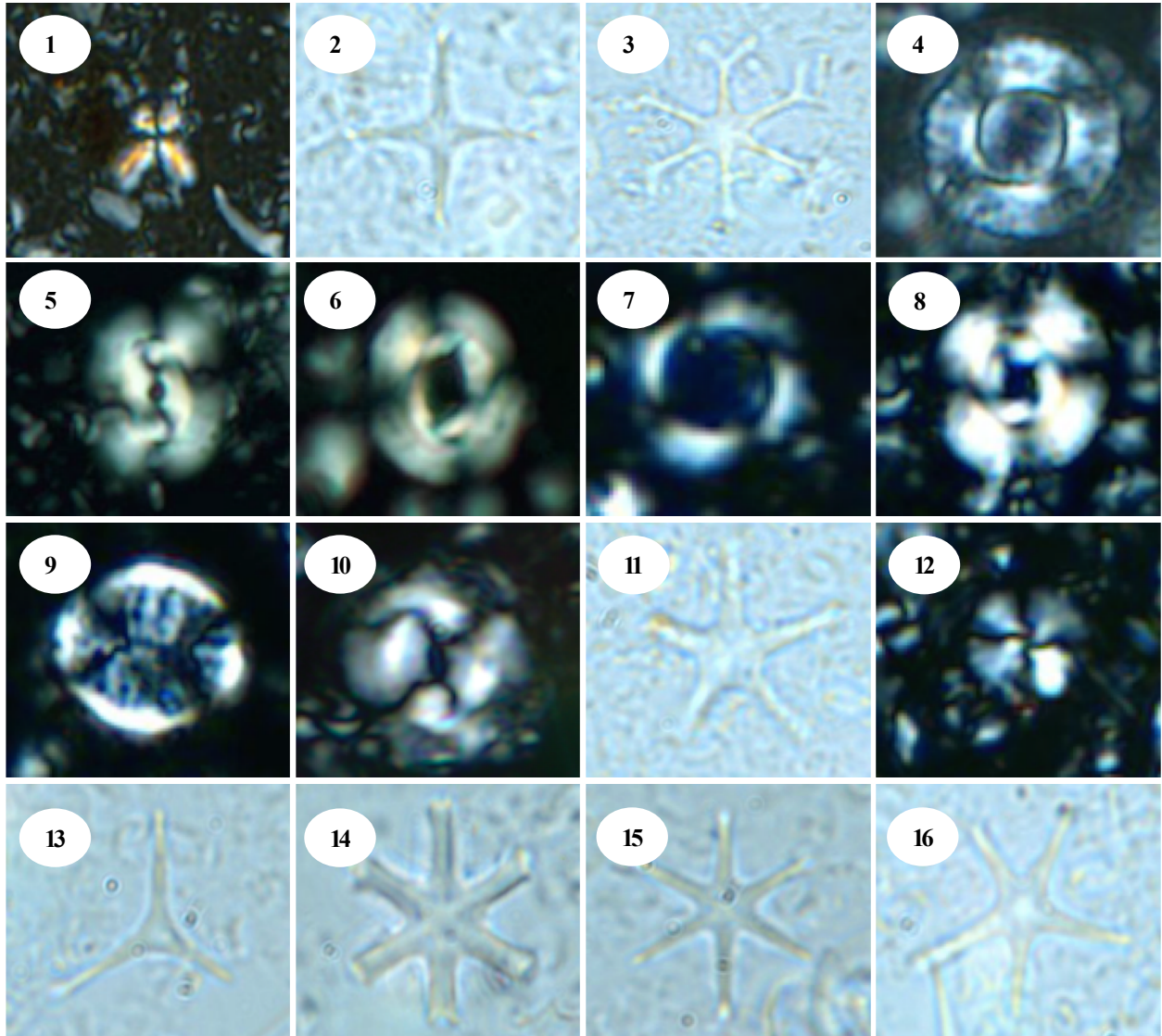


Figure 2. Examples of calcareous nannofossils that were present in the samples. 1. *Sphenolithus abies* (U1475B-18H, CC). 2. *Discoaster tamalis* (U1475B-13H-6W, 75cm). 3. *Discoaster challengeri* (U1475B-13H-6W, 75cm). 4. *Calcidiscus macintyreii* (U1475B-10H-4W, 75cm). 5. *Reticulofenestra antarcticus* (U1475B-10H-4W, 75cm). 6. *Reticulofenestra pseudoumbilicus* (U1475B-10H-4W, 75cm). 7. *Pseudoemiliana lacunosa* (U1475B-10H-4W, 75cm). 8. Reworked species (U1475B-10H-4W, 75cm). 9. *Pontosphaera* (U1475B-10H-4W, 75cm). 10. *Coccolithus pelagicus* (U1475B-9H-6W, 75cm). 11. *Discoaster pentaradiatus* (U1475B-13H-6W, 75cm). 12. *Calcidiscus leptoporus* (U1475B-10H-4W, 75cm). 13. *Discoaster triradiatus* (U1475B-13H-6W, 75cm). 14. *Discoaster surculus* (U1475B-9H-2W, 75cm). 15. *Discoaster brouweri* (U1475B-9H-2W, 75cm). 16. *Discoaster asymmetricus* (U1475B-13H-6W, 75cm).

CHAPTER II

METHODOLOGY

One objective of the International Ocean Discovery Program (IODP) Expedition 361, was to determine the dynamics of the Indian-Atlantic ocean gateway circulation during Pliocene-Pleistocene climate changes (Hall et al., 2017). Expedition 361 Site U1475 was cored on the southwestern flank of the Agulhas Plateau (41°25.61'S; 25°15.64'E), ~450 nmi south of Port Elizabeth, South Africa, in a water depth of 2669 m (Hall et al., 2017). Six holes were cored from 1.5 - 277.0 m and a total of 1015.92 m of nannoplankton ooze were recovered.

Sample Preparation

Smear slides were prepared using the Double Slurry Method (Watkins and Bergen, 2003). A Zeiss Axio Scope.A1 and a Zeiss Axioskop microscope were used for counting at x1000 magnification with plain or polarized light. A total of 50 samples were collected from the shipboard stratigraphic splice using Holes U1475B and C, from the interval between 61.403 - 88.971 m. This depth interval corresponds to an age range of ~1.90 - 3.42 Ma utilizing the shipboard age model (Hall et al., 2017). All fossils were recorded within a single field (FOV) and a transect was made across each slide until approximately 500 fossil specimens were counted from a given sample. Each FOV was completely documented. Calcareous nannoplankton were recorded at a level of individual species and 26,015 specimens were documented. See Figure 2 for examples of different nannoplankton species that are present.

***Reticulofenestra* Classification Scheme**

Reticulofenestra species were further subdivided by size and calcification. The *Reticulofenestra pseudoumbilicus* group includes *Reticulofenestra* with open central areas

(Figure 2). Specimens in the *R. pseudoumbilicus* group of maximum length measurements ≤ 3 μm , > 3 μm but ≤ 5 μm , > 5 μm but ≤ 7 μm , and > 7 μm were recorded and grouped by their size accordingly. The *Reticulofenestra antarcticus* group includes *Reticulofenestra* specimens with enclosed central areas (Figure 2). Specimens in the *R. antarcticus* group of maximum length measurements > 3 μm but ≤ 5 μm , > 5 μm but ≤ 7 μm , and > 7 μm were recorded and grouped by their size accordingly. Specimens in the *R. antarcticus* group with maximum length measurement of ≤ 3 μm were recorded in the *R. pseudoumbilicus* group as it was difficult to identify these small fossils at the species level.

Analytical Methods

Relative abundance plots were created at the genera and species level in a time series using the shipboard age model. The *Reticulofenestra* specimens were grouped as follows; all *Reticulofenestra* specimens ≤ 5 μm ; *R. pseudoumbilicus* > 5 μm ; and *R. antarcticus* > 5 μm . *Calcidiscus leptopus*, *Calcidiscus tropicus*, and *Calcidiscus macintyreii* were grouped to represent the *Calcidiscus* genera. Similarly, all *Discoaster* species were grouped to represent the *Discoaster* genera and all *Helicosphaera* species were grouped to represent the *Helicosphaera* genera.

The species richness and Shannon diversity were calculated for each sample. Species richness records the number of different species present in each sample. The Shannon diversity index is a diversity index that considers both richness and evenness. Shannon diversity index values (H) closer to 0.0 represent less diversity in the assemblage. Increasing H values represent greater diversity within the assemblage.

A temperature index was calculated for each sample. (Equation 1). Temperature index values closer to 0.0 represent relatively cooler surface waters while temperature index values

closer to 1.0 represent relatively warmer surface waters. The species and genera used in the temperature index include those known for having ecological preferences based on surface water temperatures. The warm-water species include those belonging to the genera *Discoaster* (Aubry, 1992; Gibbs et al., 2006; Villa et al. 2008), *Calcidiscus* (Di Stefano et al., 2010; Marino et al., 2011;), and *Helicosphaera* (Mcintyre et al., 1967; Ziveri et al., 2004). The cold-water species include *Coccolithus pelagicus* (Mcintyre et al., 1967; Raffi and Rio, 1981) and *Pseudoemiliana lacunosa* (Gartner, 1972; Marino et al., 2011).

$$\text{Temperature Index} = \frac{\text{Total Warm Water Species Abundance}}{\text{Total Warm Water Species Abundance} + \text{Total Cold Water Species Abundance}}$$

Equation 1. Temperature Index.

Two species rank abundance plots were created before species grouping (Equation 2). One species rank abundance plot includes the *Reticulofenestra* $\leq 5 \mu\text{m}$ signal in the total number of specimens per sample and the other excludes the *Reticulofenestra* $\leq 5 \mu\text{m}$ signal in the total number of specimens per sample.

Species Rank Abundance of Species β =

$$\frac{\text{Species } \beta \text{ Raw Count in Sample 1} + \text{Species } \beta \text{ Raw Count in Sample 2} + \dots}{\text{Total Number of Specimens in Sample 1} + \text{Total Number of Specimens in Sample 2} + \dots}$$

Equation 2. Species Rank Abundance.

An area chart was created to show the relative abundances of each species before grouping for each sample (Figure 3). The area chart includes the *Reticulofenestra* $\leq 5 \mu\text{m}$ signal.

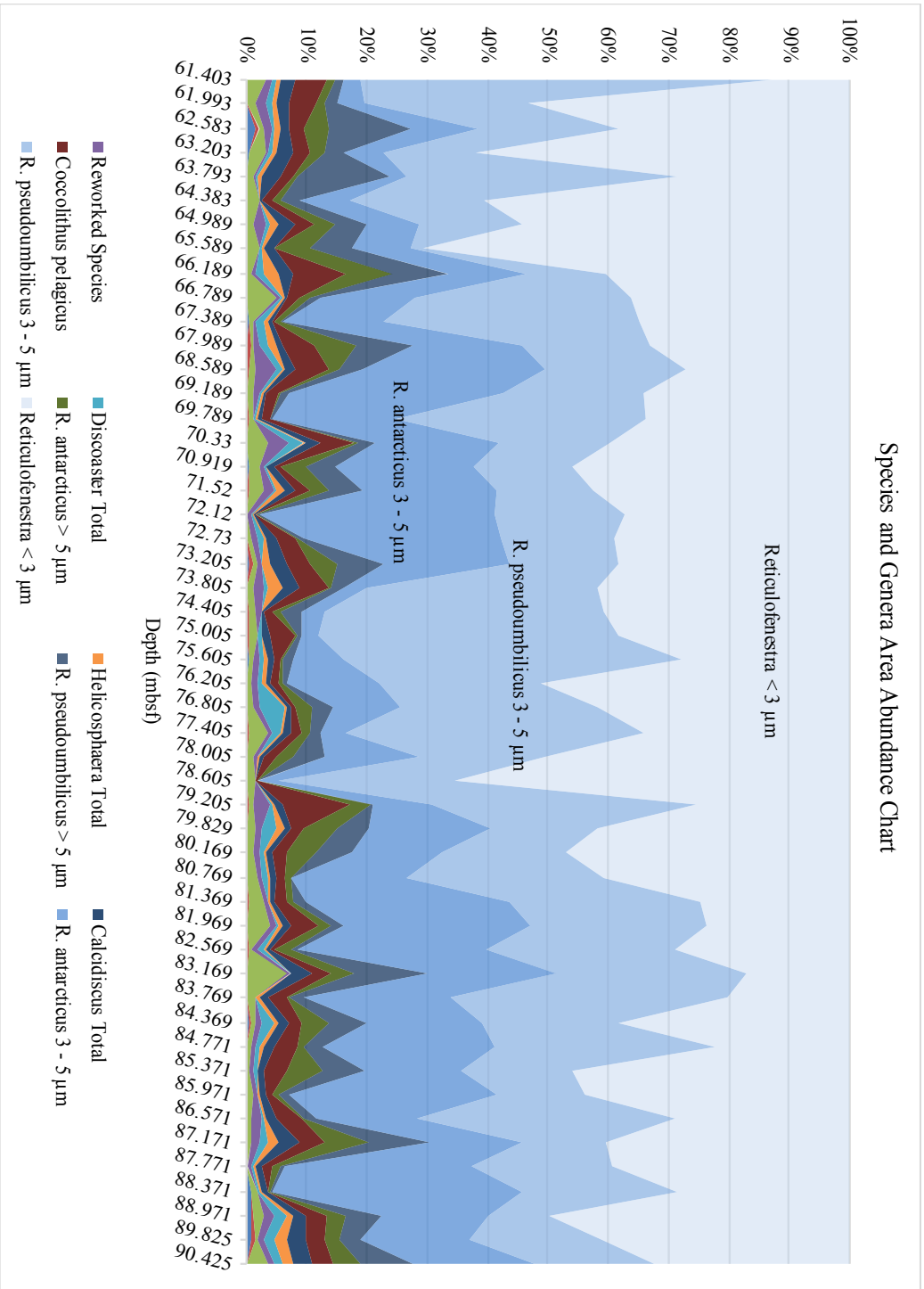


Figure 3. Species and genera area abundance plot for each sample organized by depth (mbsf).

CHAPTER III

RESULTS

Richness and Diversity

Out of the 26,015 specimens documented, a total of 25 species were identified (see Figure 2 for examples). The species richness in a given sample varies from 8 - 21 species (Figure 4). The average number of species in a given sample is 15 species. The species richness of the samples experiences increased variability from ~3.4 - 3.0 Ma with species present ranging from 10 - 21 species. From 2.89 - 2.76 Ma the species richness stays relatively consistent with ~15 species present in each sample. This is interrupted by another period of variability from 2.72 - 2.09 Ma where the species richness ranges from 8 - 21 species present in a given sample.

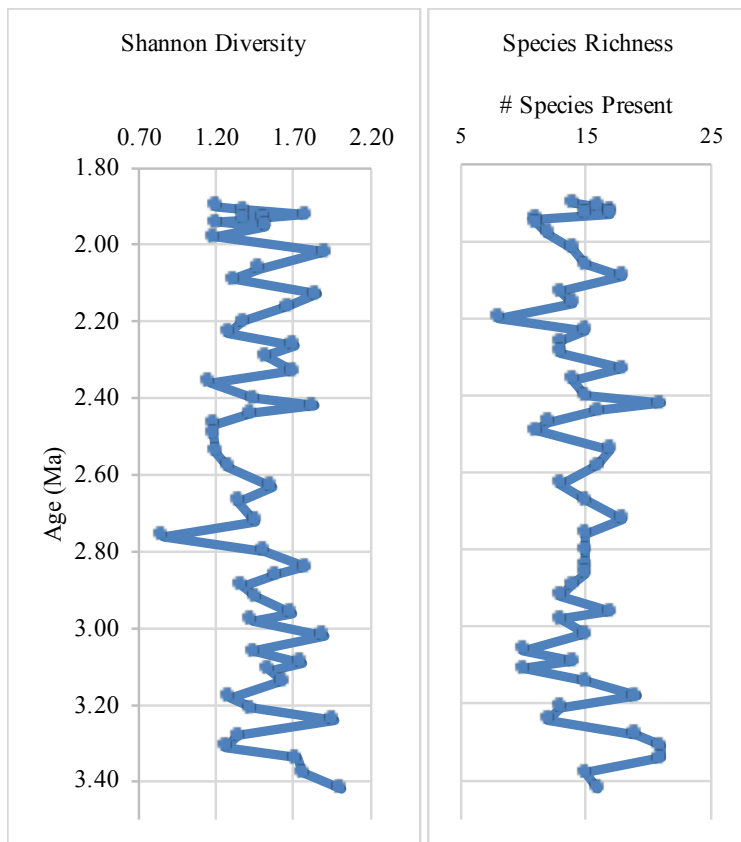


Figure 4. Shannon diversity index and species richness for each sample.

The Shannon diversity index of the assemblage has an H value range of 0.86 - 2.01 with an average H value of 1.50 (Figure 4). The assemblage experiences intervals of variability in species diversity from ~3.4 - 2.8 Ma and ~2.4 - 1.9 Ma with H values ranging from 1.2 - 2.01 during both time intervals. There is a time interval of low diversity from 2.76 - 2.47 Ma where H values ranges from 0.86 - 1.56. The Shannon diversity index appears to be primarily controlled by the abundance of *Reticulofenestra* $\leq 5 \mu\text{m}$ specimens and consequently the Shannon diversity index curve is a mirror image of the *Reticulofenestra* $\leq 5 \mu\text{m}$ curve.

Full Assemblage Details

The *Reticulofenestra* $\leq 5 \mu\text{m}$ signal dominates the assemblage and consists of 67.22 – 98.43% of the specimens in any given sample (Figure 3) and 84.93% of the total specimens documented (Figure 5a).

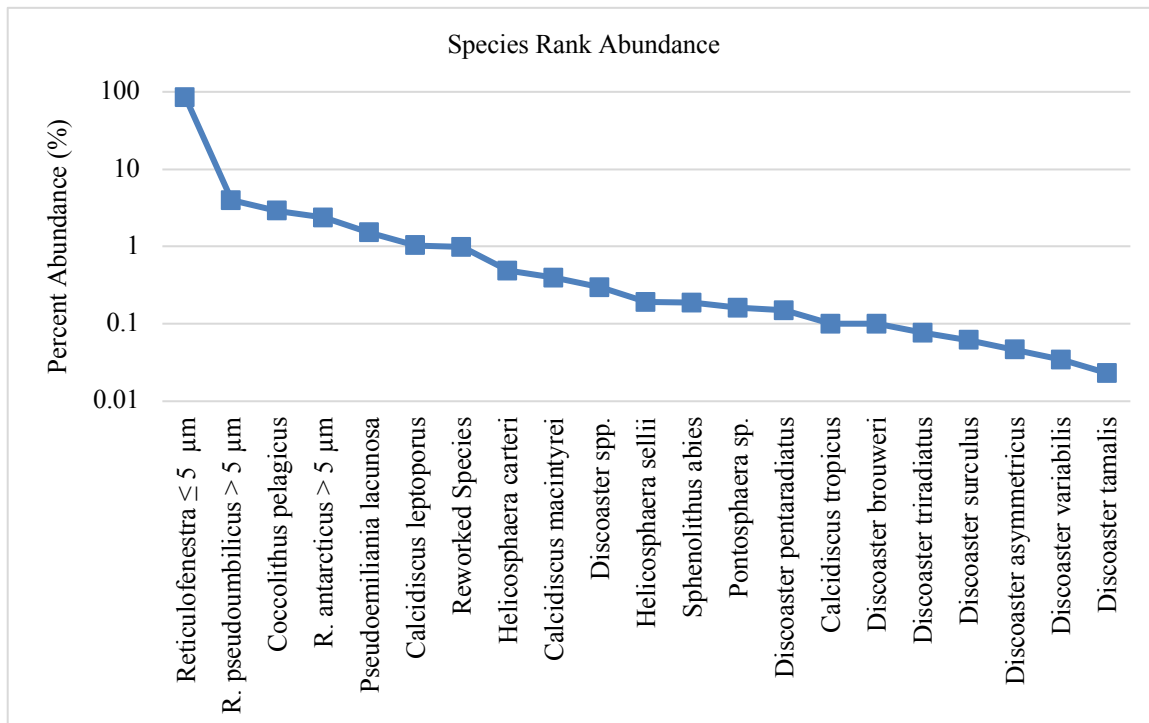


Figure 5a. Species Rank Abundance plot including the *Reticulofenestra* $\leq 5 \mu\text{m}$ signal.

The total abundance of *R. pseudoumbilicus* > 5 µm and *Coccolithus pelagicus* are 3.97% and 2.89%, respectively. *Reticulofenestra antarcticus* > 5 µm, *Pseudoemiliana lacunosa*, and *Calcidiscus leptoporus* consist of 2.37%, 1.51%, and 1.03% of the total specimens documented, respectively. The remaining species range from 0.98% to 0.02% of the total specimens documented.

Full Assemblage Details Excluding the *Reticulofenestra* ≤ 5 µm Signal

Analyzing fluctuations in the less abundant species may be more indicative of paleoenvironmental information. Similar trends were observed when including the *Reticulofenestra* ≤ 5 µm signal, therefore, the *Reticulofenestra* ≤ 5 µm signal was excluded when creating abundance plots to better observe the fluctuations and trends of the less prominent species. After removing the *Reticulofenestra* ≤ 5 µm signal from the assemblage, there are 3,921 total specimens documented, and the number of specimens in any given sample ranges from 11 – 161 specimens. The average number of specimens in any given sample is 74 specimens.

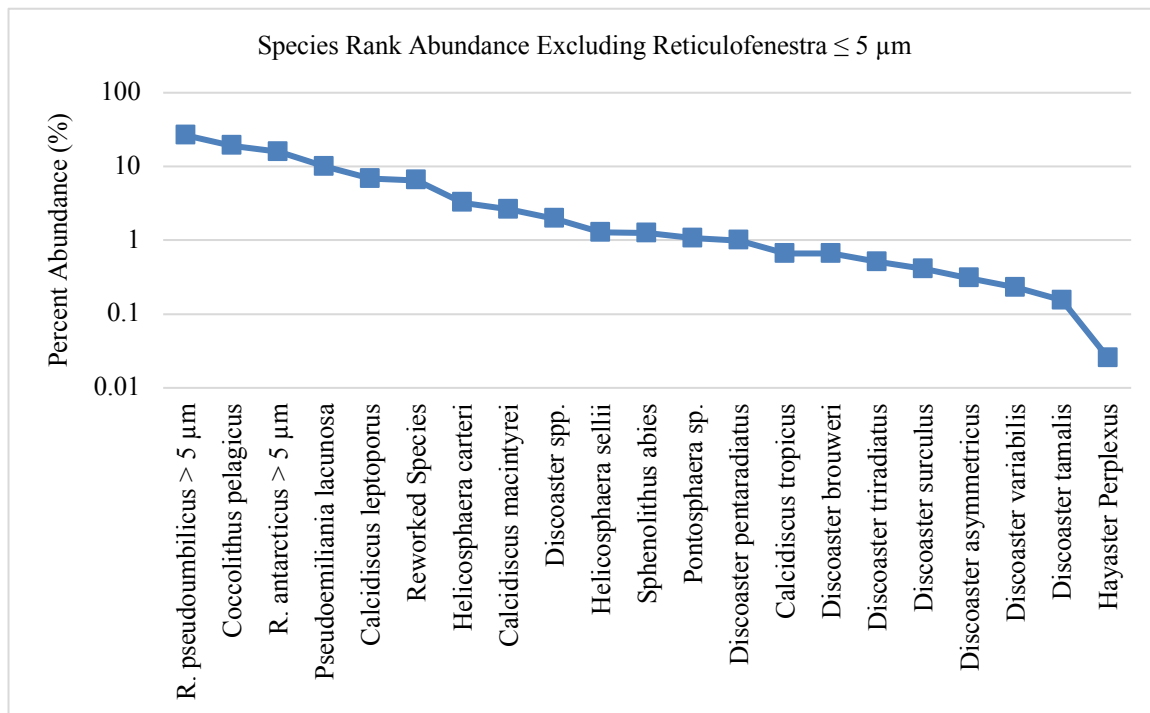


Figure 5b. Species rank abundance excluding the *Reticulofenestra* ≤ 5 µm signal.

Reticulofenestra pseudoumbilicus > 5 μm , *Coccolithus pelagicus*, and *R. antarcticus* > 5 μm compose 26.37%, 19.15%, and 15.73% of the total specimens documented, respectively (Figure 5b). *Pseudoemiliana lacunosa* and *Calcidiscus leptoporus* compose 9.99% and 6.86% of the total specimens documented, respectively. Reworked species, which are specimens that are older than the studied time interval, make up 6.50% of the total specimens documented. *Helicosphaera carteri*, and *Calcidiscus macintyreii* compose 3.23% and 2.62% of the total specimens, respectively. The remaining species range from 1.96 - 0.15% of the total specimens documented.

Individual Species and Genera Details Excluding the *Reticulofenestra* \leq 5 μm Signal

The genus *Calcidiscus* is present throughout the record and exhibits an abundance of 1.82 - 22.22% in any given sample (Figure 6a). *Calcidiscus* specimens are more commonly found from ~3.4 – 2.9 Ma.

The genus *Discoaster* exhibits intermittent absences throughout the record (Figure 6a). When present, *Discoaster* specimens have an abundance of 0.67 – 27.63% in any given sample. There are no apparent trends in the *Discoaster* record.

The genus *Helicosphaera* also exhibits intermittent absences throughout the record (Figure 6a). When present, *Helicosphaera* specimens have an abundance of 0.63 – 14.77% in any given sample. *Helicosphaera* specimens are more commonly found from ~3.4 – 3.0 Ma.

Other than a single brief absence at 2.29 Ma, *Coccolithus pelagicus* is found throughout the record with an abundance of 5.56 – 61.00% in any given sample (Figure 6a). *Coccolithus pelagicus* abundances are relatively constant through time.

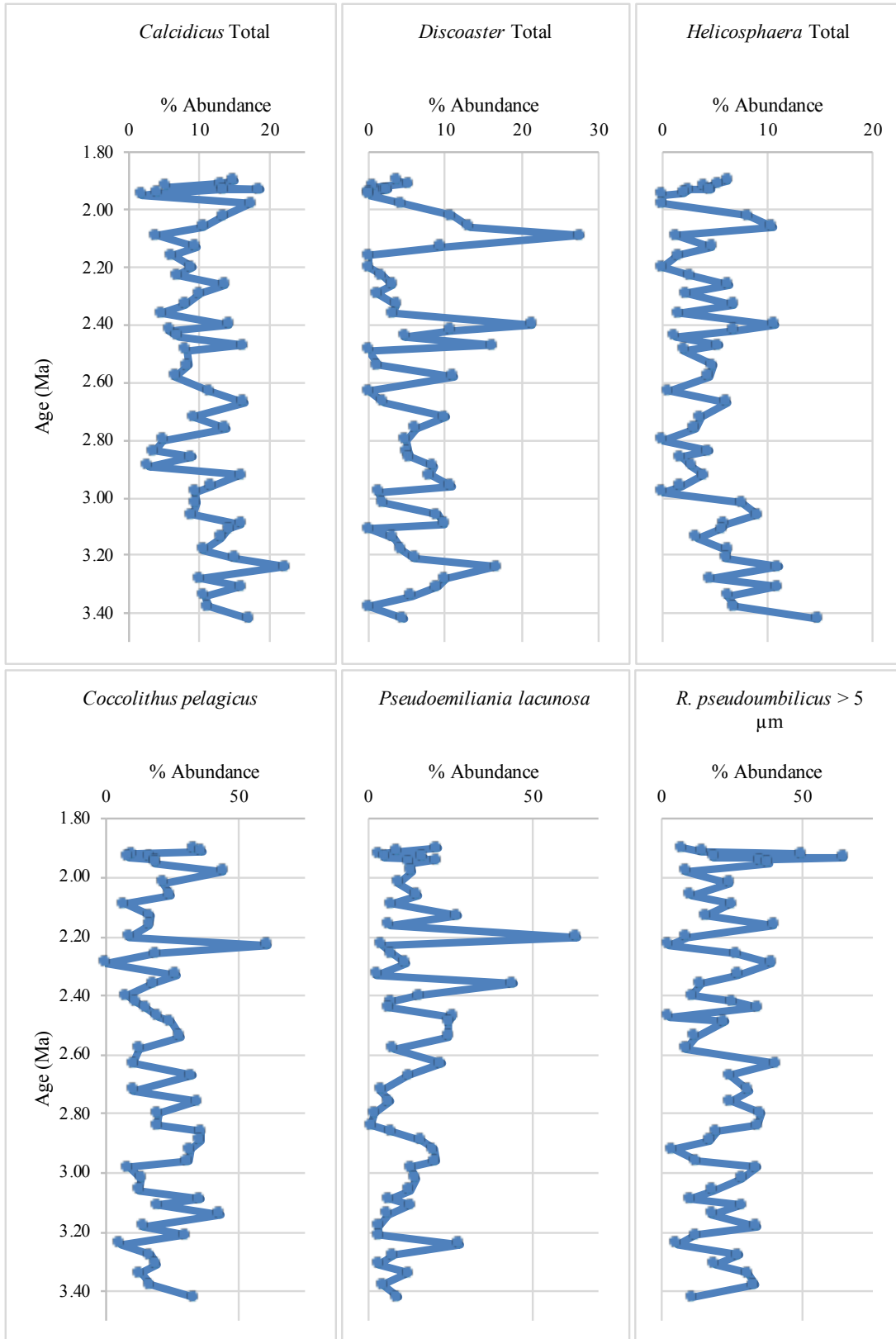


Figure 6a. Top: species and genera relative abundance plots for *Calcidiscus*, *Discoaster*, and *Helicosphaera*. Bottom: species and genera relative abundance plots for *Coccolithus pelagicus*, *Pseudoemiliana lacunosa*, and *R. pseudoumbilicus* > 5 μm .

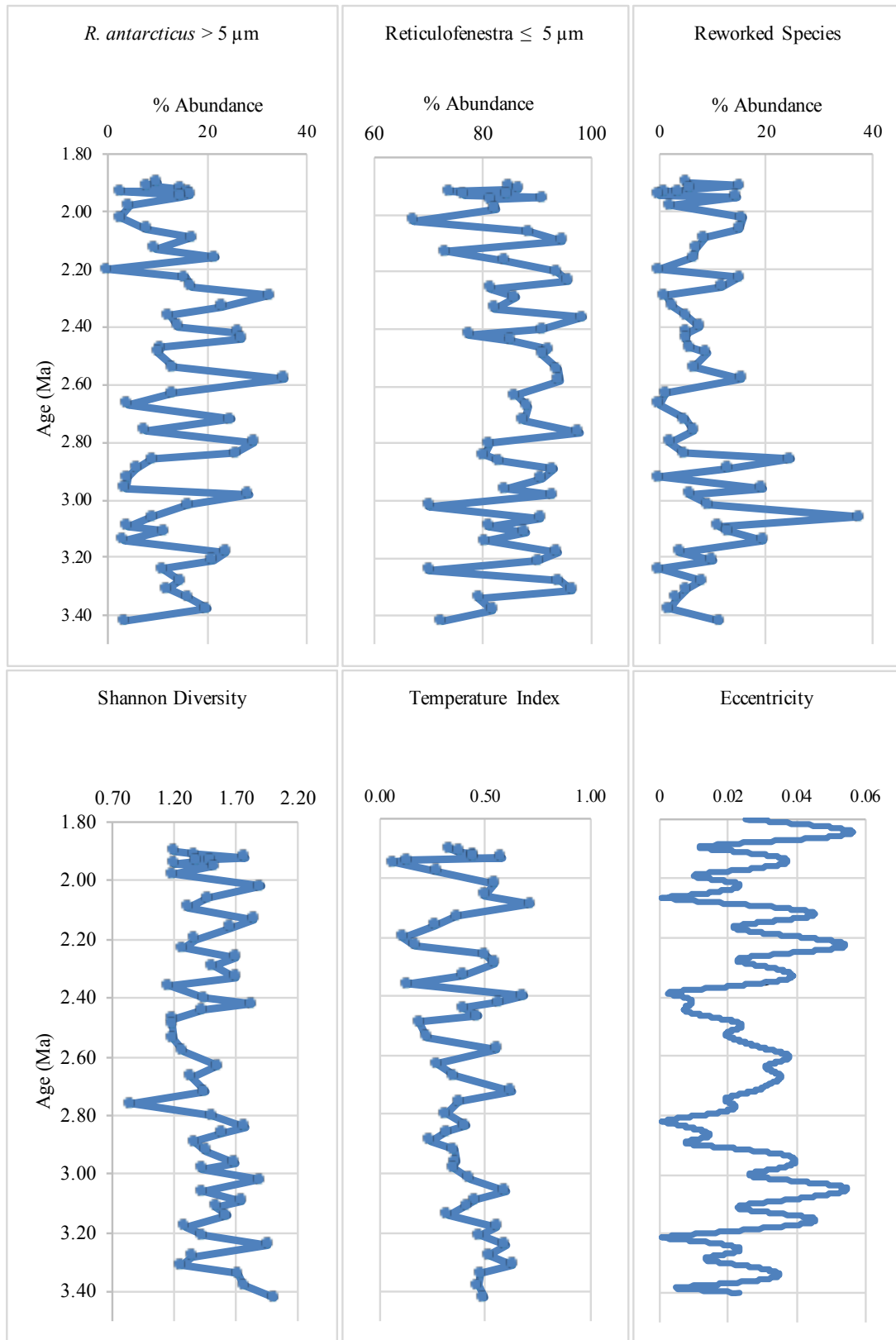


Figure 6b. Top: species and genera relative abundance plots for *Reticulofenestra antarcticus* > 5 μm, *Reticulofenestra* ≤ 5 μm, and the reworked species. Bottom: the Shannon diversity, temperature index, and global eccentricity curve (Laskar et al., 2004).

Pseudoemiliana lacunosa is found sporadically throughout the record, but when present has an abundance of 0.78 – 63.64% in any given sample (Figure 6a). This species is more commonly present from ~2.7 – 2.2 Ma.

Reticulofenestra pseudoumbilicus > 5 µm is present throughout the record and varies from 2.61 – 64.71% in any given sample (Figure 6a). There appears to be no major long-term trend in *R. pseudoumbilicus* > 5 µm abundance.

Reticulofenestra antarcticus > 5 µm is present throughout the record except for a single brief absence at 2.20 Ma (Figure 6b). When present, *R. antarcticus* > 5 µm specimens have an abundance of 2.52 – 35.56% in any given sample. *Reticulofenestra antarcticus* > 5 µm specimens are more commonly found from ~2.9 – 2.2 Ma.

Reworked species are found sporadically throughout the record and exhibit intermittent absences (Figure 6b). When present, reworked species have an abundance of 0.85 – 37.50% in any given sample. Reworked species are most commonly found from ~3.2 – 2.8 Ma.

CHAPTER IV

DISCUSSION

Nannoplankton as Environmental Indicators

Several nannoplankton species are known for their paleoenvironmental preferences due to their respective biogeography. Established by multiple studies, *Calcidiscus macintyreii* and *C. leptoporus*, *Discoaster* species, and *Helicosphaera carteri* and *H. sellii* are warm-water species (Bukry, 1978; Bach et al., 2015) and *Coccolithus pelagicus*, and *Pseudoemiliana lacunosa* are cold-water species (Geitzenauer, 1972; Robinson, 2006). The variation in relative abundances of these nannoplankton species downhole consequently reflects changes in water temperature with time.

Warm-Water Indicators

Calcidiscus and *Helicosphaera* experience a decreasing trend in abundance from ~3.4 to 3.0 Ma (Figure 6a). This decreasing trend could be a reflection of the long-term gradual cooling of the warmer Pliocene climate into the cooler Pleistocene climate and subsequent decrease in sea surface temperatures.

The warm-water genus *Helicosphaera* experiences increased variability from ~2.6 to 2.2 Ma (Figure 6a). The warm-water genera *Calcidiscus* and *Discoaster* experience similar variability increases from ~2.5 Ma to 2.3 Ma. These variability increases could be a reflection of the major glacial and interglacial cycles that begin at the onset of the PPT.

These three genera experience a sudden increase in abundance from ~2.1 – 2.0 Ma which is most prominent in *Discoaster* species at 2.1 Ma (Figure 6a). This pulse coincides with a sudden drop in the cold-water species *Pseudoemiliana lacunosa* during the same time interval.

Cold-Water Indicators

The cold-water species *Pseudoemiliana lacunosa* experiences an increase in abundance from ~3.2 – 2.9 Ma which is in the same interval that *Calcidiscus* and *Helicosphaera* experience decreasing trends (Figure 6a). *Pseudoemiliana lacunosa* displays a stepped increase in abundance from ~2.8 - 2.2 Ma across the Pliocene-Pleistocene boundary (2.58 Ma). Both of these trends may indicate a long-term cooling trend of sea surface temperatures. *Pseudoemiliana lacunosa* then experiences a sudden drop in abundance after ~2.2 Ma.

The cold-water species *Coccolithus pelagicus* exhibits a sudden pulse of increased abundance at 2.23 Ma that coincides with the maximum abundance of *Pseudoemiliana lacunosa* at the termination of its increasing trend (Figure 6a). From 3.28 – 3.06 Ma, *C. pelagicus* exhibits an increase in variability that corresponds to a similar increase in variability over the same interval in the reworked species signal.

***Reticulofenestra* ≤ 5 μm, *R. pseudoumbilicus* > 5 μm, and *R. antarcticus* > 5 μm**

Reticulofenestra pseudoumbilicus > 5 μm shows an interval of increased variability from 2.2 – 2.0 Ma (Figure 6b). *Reticulofenestra antarcticus* > 5 μm does not experience any observable long-term trends. *Reticulofenestra* ≤ 5 μm experiences increased variability from ~3.4 - 2.8 Ma. In addition, from ~2.8 - 2.4 Ma *Reticulofenestra* ≤ 5 μm experiences sustained high abundance.

Environmental Change Across the Pliocene-Pleistocene Transition

The temperature index experiences somewhat constant values slightly above 0.5 from ~3.4 – 3.2 Ma which may reflect a more stable Pliocene climate (Figure 6b). Temperature index maxima values increase from 0.60 at ~3.24 Ma to 0.71 at 2.0 Ma. Temperature index minima dramatically decrease in value from 0.32 at 3.14 Ma to 0.06 at 1.9 Ma, which may reflect a major

long-term cooling trend across the PPT from ~3.2 – 1.9 Ma. The temperature index also experiences a progressive increase in variability from ~2.8 – 1.9 Ma that could be a reflection of the major glacial and interglacial cycles that began at ~2.7 Ma.

It is recognized that the Earth's orbital configuration has an influence on climate. The Earth's orbit around the sun takes the shape of an ellipse. The amount of deviation from a perfect circle the Earth's orbit experiences varies on cycles of 100,000 and 400,000 years and is measured by its eccentricity. Eccentricity cycles can change annual mean insolation rates by ~0.2% and this insolation change is thought to not have noticeable effects to earth's climate (Nisancioglu, 2009). Benthic $\delta^{18}\text{O}$ records have expressed 41 kyr obliquity forced cycles during the late Pliocene to the early Pleistocene (3.0 – 0.8 Ma) with poorly understood 100 kyr appearing only recently at ~0.8 Ma (Lisiecki & Raymo, 2007). These cycles are thought to be climate drivers and major contributors to the occurrence of glacial and interglacial cycles. Here we compare the temperature index and assemblage trends to the eccentricity signal rather than to obliquity. The sample resolution for the nannoplankton data is too coarse to confidently examine for 41 kyr cyclicality.

When comparing the temperature index with eccentricity, from ~2.72 to 1.9 Ma the temperature index appears to follow the eccentricity signal on broad ~400 kyr cycles. Most noticeably, the temperature index shows peak warm values at 2.72, 2.40 and 2.09 Ma that correspond to eccentricity minima at roughly the same time intervals. This correlation could possibly reflect a poorly understood eccentricity driven climate signal corresponding to latitudinal frontal migration patterns or sea surface temperature variations due to global temperature fluctuations on ~400 kyr cycles.

The temperature index also seems to have a less prominent background signal on ~200 kyr cycles beginning at ~2.8 – 2.7 Ma. This background signal yields less warm peaks at 2.58 and 2.29 Ma set between the three warm maxima and does not appear to be obviously expressed in the eccentricity signal. This signal could be further explored by increasing the sampling resolution.

The broad ~400 kyr cycles begin in the temperature index at 2.72 Ma, around the same time major Northern Hemisphere glaciation is thought to have occurred (Maslin et al., 1998). The onset of Northern Hemisphere glaciation appears to introduce the subsequent long-term cooling trend and variability increase observed in the temperature index. Latitudinal migrations of the subtropical front at 2.72 Ma may have catapulted the globe into major Northern hemisphere glaciation, and the subsequent global cooling and glacial cycles could be expressed in the long-term cooling and variability trends of the temperature index. These temperature index trends could therefore be indicative of stationary cooling of sea surface waters or the incursion of cooler waters from the latitudinal migration of the Southern Ocean Fronts due to Antarctic ice sheet expansion.

CHAPTER V

CONCLUSION

The observable trends in the nanoplankton assemblage suggest surface waters cooled across the PPT. The onset of Northern hemisphere glaciation at ~2.7 Ma appears to have noticeable effects on the temperature index. The cooling trends exhibited by the temperature index could be indicative of (1) stationary cooling of surface waters due to gradual global cooling and the subsequent onset of glacial intervals beginning at the PPT and/or (2) cooling surface waters due to the incursion of northward migrating Subtropical frontal zones due to expanding Antarctic ice sheets. The intervals of increased variability experienced by the temperature index at ~2.8 Ma may reflect major glacial and interglacial periods and could possibly be linked to the global eccentricity on ~400 kyr cycles. This potentially challenges our current understanding of Milankovitch forced climate signals during the late Pliocene and early Pleistocene. In addition, the sustained high abundance of *Reticulofenestra* $\leq 5 \mu\text{m}$, the subsequent sustained low abundance of *R. pseudoumbilicus* $> 5 \mu\text{m}$ and *R. antarcticus* $> 5 \mu\text{m}$, and the termination of the high variability in most species and genera abundances at ~2.2 - 1.95 Ma may further reflect higher surface water production during this interval.

REFERENCES

- Aubry, M-P. (1992). 26. Paleogene calcareous nannofossils from the Kerguelen Plateau, Leg 120. *Proceedings of the Ocean Drilling Program, Scientific Results*, 120, 471-491. <https://doi.org/10.2973/odp.proc.sr.120.149.1992>
- Bach, L. T., Riebesell, U., Gutowska, M. A., Federwisch, L., & Schulz, K. G. (In Press) A unifying concept of coccolithophore sensitivity to changing carbonate chemistry embedded in an ecological framework. *Progress in Oceanography*. <http://dx.doi.org/10.1016/j.pocean.2015.04.012>
- Bard, E., & Rickaby, R. E. M. (2009). Migration of the subtropical front as a modulator of glacial climate. *Nature*, 460, 380-384. <https://doi.org/10.1038/nature08189>
- Bartoli, G., Hönisch, B., & Zeebe, R. E. (2011). Atmospheric CO₂ decline during the Pliocene intensification of Northern Hemisphere glaciations. *Paleoceanography*, 26, 4213- 4217. <https://doi.org/10.1029/2010PA002055>
- Barrett, P. J., Adams, C. J., McIntosh, W. C., Wisner III, C. C., & Wilson, G. S. (1992). Geochronological evidence supporting Antarctic deglaciation three million years ago. *Nature*, 359, 816-818. <https://doi.org/10.1038/359816a0>
- Bukry, D. (1978). Cenozoic coccolith, silicoflagellate, and diatom stratigraphy, Deep Sea Drilling Project Leg 44. *Deep Sea Drilling Project Initial Reports* (Vol. 44, pp. 807-863). College Station, TX: International Ocean Discovery Program. <https://doi.org/10.2973/dsdp.proc.44.137.1978>
- Cronin, T. M. (1991). Pliocene shallow water paleoceanography of the North Atlantic Ocean based on marine ostracodes. *Quaternary Science Review*, 10, 175–188. [https://doi.org/10.1016/0277-3791\(91\)90017-O](https://doi.org/10.1016/0277-3791(91)90017-O)
- Di Stefano, A., Verducci, M., Lirer, F., Ferraro, L., Iaccarino, S. M., Hüsing, S. K., & Hilgen, F. J. (2010). Paleoenvironmental conditions preceding the Messinian Salinity Crisis in the Central Mediterranean: Integrated data from the Upper Miocene Trave section (Italy). *Palaeogeography, Palaeoclimatology, Palaeoecology*, 297, 37-53. <https://doi.org/10.1016/j.palaeo.2010.07.012>

- Gartner, S., (1972). Late Pleistocene calcareous nannofossils in the Caribbean and their interoceanic correlation. *Palaeogeography, Palaeoclimatology, Palaeoecology*, 12, 169-191. [https://doi.org/10.1016/0031-0182\(72\)90058-2](https://doi.org/10.1016/0031-0182(72)90058-2)
- Geitzenauer, K. R. (1972). The Pleistocene calcareous nannoplankton of the subantarctic Pacific Ocean. *Deep-Sea Research*, 19, 45-60. [https://doi.org/10.1016/0011-7471\(72\)90072-1](https://doi.org/10.1016/0011-7471(72)90072-1)
- Gibbs, S. J., Brown, P. R., Sessa, J. A., Bralower, T. J., & Wilson, P.A. (2006). Nannoplankton Extinction and Origination Across the Paleocene-Eocene Thermal Maximum. *Science*, 324, 1770-1773. <https://doi.org/10.1126/science.1133902>
- Hall, I. R., Hemming, S. R., LeVay, L. J. and the Expedition 361 Scientists. (2017). *South African Climates (Agulhas LGM Density Profile)*. Proceedings of the International Ocean Discovery Program, 361: College Station, TX: International Ocean Discovery Program. <https://doi.org/10.14379/iodp.proc.361.2017>
- Laskar, J., Robutel, P., Joutel, F., Gastineau, M., Correia, A. C. M., Levrard, B. (2004). A long term numerical solution for the insolation quantities of the Earth. *A&A*, 428, 261-285. <https://doi.org/10.1051/0004-6361:20041335>
- Lisiecki, L. E., and M. E. Raymo (2007), Plio-Pleistocene climate evolution: Trends and transitions in glacial cycle dynamics. *Quaternary Science Reviews*, 26, 56-69 <https://doi.org/10.1016/j.quascirev.2006.09.005>
- Marino, M., Maiorano, P., Lirer, F., & Pelosi, N. (2009). Response of calcareous nannofossil assemblages to paleoenvironmental changes through the mid-Pleistocene revolution at Site 1090 (Southern Ocean). *Palaeogeography, Palaeoclimatology, Palaeoecology*, 280, 333-349. <https://doi.org/10.1016/j.palaeo.2009.06.019>
- Marino, M., Maiorano, P., & Flower, B. P. (2011). Calcareous nannofossil changes during the Mid-Pleistocene Revolution: Paleoecologic and paleoceanographic evidence from North Atlantic Site 980/981. *Palaeogeography, Palaeoclimatology, Palaeoecology*, 306, 58-69. <https://doi.org/10.1016/j.palaeo.2011.03.028>
- Maslin, M. A., Li, X. S., Loutre, M-F., Berger, A. (1998) The contribution of orbital forcing to the progressive intensification of northern hemisphere glaciation. *Quaternary Science Reviews*, 17, 411-426. [https://doi.org/10.1016/s0277-3791\(97\)00047-4](https://doi.org/10.1016/s0277-3791(97)00047-4).

- Marlow, J. R., Lange, C. B., Wefer, G., & Rosell-Melé, A. (2000). Upwelling intensification as part of the Pliocene-Pleistocene climate transition. *Science*, 290, 2288-2291. <https://doi.org/10.1126/science.290.5500.2288>
- McIntyre, A., & Bé, A. H. (1967). Modern Coccolithophoridae of the Atlantic Ocean—I. Placoliths and Cyrtoliths. *Deep Sea Research*, 14, 561-597. [https://doi.org/10.1016/0011-7471\(67\)90065-4](https://doi.org/10.1016/0011-7471(67)90065-4)
- McKay, R., Naish, T., Carter, L., Riesselman, C., Dunbar, R., Sjunneskog, C., Winter, D., Sangiorgi, F., et al. (2012). Antarctic and Southern Ocean influences on Late Pliocene global cooling. *PNAS*, 109, 6423-6428. <https://doi.org/10.1073/pnas.1112248109/-/DCSupplemental>.
- Nisancioglu, K. H. (2010) Plio-Pleistocene Glacial Cycles and Milankovitch Variability. *Encyclopedia of Ocean Sciences*, 504-513. <https://doi.org/10.1016/B978-012374473-9.00702-5>
- Raffi, I., & Rio, D. (1981). *Coccolithus pelagicus* (Wallich): a paleotemperature indicator in the late Pliocene Mediterranean deep sea record. In Wezel, F.C. (Ed.), *Sedimentary Basins of Mediterranean Margins: C.N.R. Italian Project of Oceanography*, Bologna (Tecnoprint), 187–190.
- Ravelo, A. C., Andreason, D. H., Lyle, M., Lyle, A. O., & Wara, M. W. (2004). Regional climate shifts caused by gradual global cooling in the Pliocene epoch. *Nature*, 429, 263-267. <https://doi.org/10.1038/nature02567>
- Raymo, M. E., Grant, B., Horowitz, M., & Rau, G. H. (1996). Mid-Pliocene warmth: stronger greenhouse and stronger conveyor. *Marine Micropaleontology*, 27, 313-326. [https://doi.org/10.1016/0377-8398\(95\)00048-8](https://doi.org/10.1016/0377-8398(95)00048-8)
- Robinson, A. R., & Brink, K. H. (2005). *The Global Coastal Ocean - Regional Studies and Syntheses*. (Vol. 11). Cambridge, MA: The Harvard University Press.
- Romero, O. E., Kim, J.-H., Barcena, M. A., Hall, I. R., Zahn, R., & Schneider, R. (2015). High-latitude forcing of diatom productivity in the southern Agulhas Plateau during the past 350kyr. *Paleoceanography*, 30, 118-132. <https://doi.org/10.1002/2014PA002636>

- Sosdian, S., & Rosenthal, Y. (2009). Deep-Sea Temperature and Ice Volume Changes Across the Pliocene-Pleistocene Climate Transitions. *Science*, 325, 306-310. <https://doi.org/10.1126/science.1169938>
- Villa, G., Fioroni, C., Pea, L., Bohaty, S., & Persico, D. (2008). Middle Eocene–late Oligocene climate variability: Calcareous nannofossil response at Kerguelen Plateau, Site 748. *Marine Micropaleontology*, 69, 173-192. <https://doi.org/10.1016/j.marmicro.2008.07.006>
- Watkins, D. K., & Bergen, J. A. (2003). Late Albian adaptive radiation in the calcareous nannofossil genus *Eiffellithus*. *Micropaleontology*, 49, 232-252. <https://doi.org/10.2113/49.3.231>
- Weier, J. (1999). What is a Coccolithophore? Fact Sheet: Feature Articles. *NASA Earth Observatory*. Retrieved from earthobservatory.nasa.gov/Features/Coccolithophores/
- Ziegler, M., Diz, P., Hall, I. R., & Zahn, R. (2013). Millennial-scale changes in atmospheric CO₂ levels linked to the Southern Ocean carbon isotope gradient and dust flux. *Nature Geoscience*, 6, 457-461. <https://doi.org/10.1038/NGEO1782>
- Ziveri, P., Baumann, K-H., Bockel, B., Bollmann, J., & Young, J. R. (2004). Biogeography of selected Holocene coccoliths in the Atlantic Ocean. *Coccolithophores: From Molecular Processes to Global Impact*, 403-428. https://doi.org/10.1007/978-3-662-06278-4_15

Table 2a. Species relative abundance counts for each sample throughout the record. International Ocean Discovery Program, Expedition 361, Site U1475.

Hole, Core, Type, Section, A/W	Top Interval (cm)	Bottom Interval (cm)	Top depth CCSF (m)	Age	<i>Calcidiscus leptoporus</i>	<i>Calcidiscus macintyreii</i>	<i>Calcidiscus tropicus</i>	<i>Coccolithus pelagicus</i>	<i>Discoaster asymmetricus</i>	<i>Discoaster brouweri</i>	<i>Discoaster pentaradiatus</i>	<i>Discoaster surculus</i>	<i>Discoaster tamalis</i>	<i>Discoaster triradiatus</i>	<i>Discoaster variabilis</i>	<i>Discoaster spp.</i>	<i>Hayaster perplexus</i>	<i>Helicosphaera carteri</i>	<i>Helicosphaera sellii</i>	<i>Pontosphaera sp.</i>	<i>Pseudoemiliana lacunosa</i>	<i>Reticulofenestra</i> 5-7 μ m	<i>Reticulofenestra</i> >7 μ m	<i>Reticulofenestra antarcticus</i> 5-7 μ m	<i>Reticulofenestra antarcticus</i> >7 μ m	<i>Sphenolithus abies</i>	Reworked Species	
B 7H-3W	61	62	61.4	1.90	12.5	1.3	1.3	31.3								3.8		6.3		1.3	20.0	6.3	1.3	10.0	3.9	3.9	1.3	5.0
B 7H-4W	29	30	62.6	1.92	4.0	0.7	0.7	9.4		1.3	0.7					2.6		3.4	0.7	5.4	3.4	46.3	3.4	12.8	2.0	2.0	5.4	
B 7H-5W	0	1	63.8	1.93	8.4	2.5	2.5	8.4	0.8		0.8			2.3		0.8		1.7	0.8	3.5	5.0	63.0	1.7	1.7	0.8		0.8	
B 7H-3W	1	2	70.3	2.26	1.8			16.4										2.1			20.8	35.4	14.6	2.1	2.1		2.1	
B 8H-3W	60	61	70.9	2.29	17.4			43.5				2.2				2.2					10.9	34.5	3.6	9.1	5.5	5.5	12.7	
B 8H-4W	120	121	71.5	2.33	10.8		2.7	18.9						2.7		8.1		2.7	5.4		13.0	6.5	2.2	4.3			6.5	2.2
B 8H-5W	30	31	72.1	2.36	7.9	2.6		21.1		2.6	2.6			7.9		3.9		10.5		2.6	8.1	18.9	5.4	2.7				13.5
B 9H-2W	146	147	79.8	2.84	4.8	4.8		15.9						2.6		9.5		4.8		2.6	6.6	22.4	2.6	15.8	1.3	1.3	7.9	
B 9H-3W	30	31	80.2	2.86	4.6	1.5		15.4										1.5		1.5	6.2	35.4	4.6	16.9	4.6	1.5	6.2	
B 9H-4W	60	61	81.4	2.92	6.1	0.9		53.0		0.9						0.9					3.5	1.7	0.9	14.8	0.9	0.9	13.0	
B 9H-5W	30	31	82.2	2.96	10.5	3.2		16.8								3.2		2.6	6.3	2.2	6.3	24.2	2.1	14.7	2.1		10.5	
B 9H-6W	0	1	84.4	3.09	7.1	3.6	3.6	7.1								1.1		1.5		2.2	11.2	27.0	12.4	23.6	9.0		1.1	
B 9H-3W	0	1	89.8	3.38	1.9	3.9		10.7	0.6	1.9	0.6					0.6		1.3		2.2	11.2	27.0	12.4	23.6	9.0		1.1	
B 9H-4W	60	61	90.4	3.42	4.7	2.4		14.1	0.6	1.9	0.6					0.6		1.3		2.2	11.2	27.0	12.4	23.6	9.0		1.1	
B 9H-5W	90	91	83.8	3.06	3.1	1.6		17.2	1.6							0.0		4.8		2.6	6.6	22.4	2.6	15.8	1.3	1.3	7.9	
B 10H-3W	0	1	89.8	3.38	1.9	3.9		10.7	0.6	1.9	0.6					0.6		1.3		2.2	11.2	27.0	12.4	23.6	9.0		1.1	
B 10H-4W	60	61	90.4	3.42	4.7	2.4		14.1	0.6	1.9	0.6					0.6		1.3		2.2	11.2	27.0	12.4	23.6	9.0		1.1	
B 10H-5W	90	91	83.8	3.06	3.1	1.6		17.2	1.6							0.0		4.8		2.6	6.6	22.4	2.6	15.8	1.3	1.3	7.9	
C 7H-3W	0	1	65.0	1.95	13.5		2.7	18.9			1.2					1.2		2.1		2.2	11.2	27.0	12.4	23.6	9.0		1.1	
C 7H-4W	30	31	66.8	2.06	4.4	2.2		11.1			1.2					1.2		2.1		2.2	11.2	27.0	12.4	23.6	9.0		1.1	
C 7H-5W	0	1	68.0	2.13	8.2	2.0	6.1	32.7			1.2					1.2		2.1		2.2	11.2	27.0	12.4	23.6	9.0		1.1	
C 7H-3W	60	61	65.6	1.98	8.2		2.7	18.9			1.2					1.2		2.1		2.2	11.2	27.0	12.4	23.6	9.0		1.1	
C 7H-4W	90	91	67.4	2.09	8.2	3.2		10.1			1.2					1.2		2.1		2.2	11.2	27.0	12.4	23.6	9.0		1.1	
C 7H-5W	60	61	68.6	2.16	3.7	5.5		10.1	2.8		1.2					1.2		2.1		2.2	11.2	27.0	12.4	23.6	9.0		1.1	
C 7H-3W	60	61	65.6	1.98	8.2		2.7	18.9			1.2					1.2		2.1		2.2	11.2	27.0	12.4	23.6	9.0		1.1	
C 7H-4W	90	91	67.4	2.09	8.2	3.2		10.1			1.2					1.2		2.1		2.2	11.2	27.0	12.4	23.6	9.0		1.1	
C 7H-5W	60	61	68.6	2.16	3.7	5.5		10.1	2.8		1.2					1.2		2.1		2.2	11.2	27.0	12.4	23.6	9.0		1.1	
C 7H-3W	60	61	65.6	1.98	8.2		2.7	18.9			1.2					1.2		2.1		2.2	11.2	27.0	12.4	23.6	9.0		1.1	
C 7H-4W	90	91	67.4	2.09	8.2	3.2		10.1			1.2					1.2		2.1		2.2	11.2	27.0	12.4	23.6	9.0		1.1	
C 7H-5W	60	61	68.6	2.16	3.7	5.5		10.1	2.8		1.2					1.2		2.1		2.2	11.2	27.0	12.4	23.6	9.0		1.1	
C 7H-3W	60	61	65.6	1.98	8.2		2.7	18.9			1.2					1.2		2.1		2.2	11.2	27.0	12.4	23.6	9.0		1.1	
C 7H-4W	90	91	67.4	2.09	8.2	3.2		10.1			1.2					1.2		2.1		2.2	11.2	27.0	12.4	23.6	9.0		1.1	
C 7H-5W	60	61	68.6	2.16	3.7	5.5		10.1	2.8		1.2					1.2		2.1		2.2	11.2	27.0	12.4	23.6	9.0		1.1	
C 7H-3W	60	61	65.6	1.98	8.2		2.7	18.9			1.2					1.2		2.1		2.2	11.2	27.0	12.4	23.6	9.0		1.1	
C 7H-4W	90	91	67.4	2.09	8.2	3.2		10.1			1.2					1.2		2.1		2.2	11.2	27.0	12.4	23.6	9.0		1.1	
C 7H-5W	60	61	68.6	2.16	3.7	5.5		10.1	2.8		1.2					1.2		2.1		2.2	11.2	27.0	12.4	23.6	9.0		1.1	
C 7H-3W	60	61	65.6	1.98	8.2		2.7	18.9			1.2					1.2		2.1		2.2	11.2	27.0	12.4	23.6	9.0		1.1	
C 7H-4W	90	91	67.4	2.09	8.2	3.2		10.1			1.2					1.2		2.1		2.2	11.2	27.0	12.4	23.6	9.0		1.1	
C 7H-5W	60	61	68.6	2.16	3.7	5.5		10.1	2.8		1.2					1.2		2.1		2.2	11.2	27.0	12.4	23.6	9.0		1.1	
C 7H-3W	60	61	65.6	1.98	8.2		2.7	18.9			1.2					1.2		2.1		2.2	11.2	27.0	12.4	23.6	9.0		1.1	
C 7H-4W	90	91	67.4	2.09	8.2	3.2		10.1			1.2					1.2		2.1		2.2	11.2	27.0	12.4	23.6	9.0		1.1	
C 7H-5W	60	61	68.6	2.16	3.7	5.5		10.1	2.8		1.2					1.2		2.1		2.2	11.2	27.0	12.4	23.6	9.0		1.1	
C 7H-3W	60	61	65.6	1.98	8.2		2.7	18.9			1.2					1.2		2.1		2.2	11.2	27.0	12.4	23.6	9.0		1.1	
C 7H-4W	90	91	67.4	2.09	8.2	3.2		10.1			1.2					1.2		2.1		2.2	11.2	27.0	12.4	23.6	9.0		1.1	
C 7H-5W	60	61	68.6	2.16	3.7	5.5		10.1	2.8		1.2					1.2		2.1		2.2	11.2	27.0	12.4	23.6	9.0		1.1	
C 7H-3W	60	61	65.6	1.98	8.2		2.7	18.9			1.2					1.2		2.1		2.2	11.2	27.0	12.4	23.6	9.0		1.1	
C 7H-4W	90	91	67.4	2.09	8.2	3.2		10.1			1.2					1.2		2.1		2.2	11.2	27.0	12.4	23.6	9.0		1.1	
C 7H-5W	60	61	68.6	2.16	3.7	5.5		10.1	2.8		1.2					1.2		2.1		2.2	11.2	27.0	12.4	23.6	9.0		1.1	
C 7H-3W	60	61	65.6	1.98	8.2		2.7	18.9			1.2					1.2		2.1		2.2	11.2	27.0	12.4	23.6	9.0		1.1	
C 7H-4W	90	91	67.4	2.09	8.2	3.2		10.1			1.2					1.2		2.1		2.2	11.2	27.0	12.4	23.6	9.0		1.1	
C 7H-5W	60	61	68.6	2.16	3.7	5.5		10.1	2.8		1.2					1.2		2.1		2.2	11.2	27.0	12.4	23.6	9.0		1.1	
C 7H-3W	60	61	65.6	1.98	8.2		2.7	18.9			1.2					1.2	</											

Table 2b. Species relative abundance counts for each sample throughout the record. International Ocean Discovery Program, Expedition 361, Site U1475.

Hole, Core, Type, Section, A/W	Top Interval (cm)	Bottom Interval (cm)	Top depth CCSF (m)	Age	<i>Calcidiscus leptoporus</i>	<i>Calcidiscus macintyreii</i>	<i>Calcidiscus tropicus</i>	<i>Coccolithus pelagicus</i>	<i>Discoaster asymmetricus</i>	<i>Discoaster brouweri</i>	<i>Discoaster pentaradiatus</i>	<i>Discoaster surculus</i>	<i>Discoaster tamalis</i>	<i>Discoaster triradiatus</i>	<i>Discoaster variabilis</i>	<i>Discoaster spp.</i>	<i>Hayaster perplexus</i>	<i>Helicosphaera carteri</i>	<i>Helicosphaera sellii</i>	<i>Pontosphaera sp.</i>	<i>Pseudoemiliania lacunosa</i>	<i>Reticulofenestra</i> 5-7 μ m	<i>Reticulofenestra</i> >7 μ m	<i>Reticulofenestra antarcticus</i> 5-7 μ m	<i>Reticulofenestra antarcticus</i> >7 μ m	<i>Sphenolithus abies</i>	Reworked Species
C 7H-5W	120	121	69.2	2.20	10.8			32.3	1.0	2.9					1.5			3.1	1.5	1.0	6.2	24.6		6.2	1.5		6.2
C 7H-6W	30	31	69.8	2.23		4.9		19.6	1.0	2.9					1.0	1.0		4.4	1.5	1.0	2.0	31.4	3.9	25.5	3.9	1.0	2.0
C 8H-2W	0	1	73.2	2.42	1.5	2.2		18.5		1.5	3.7							4.4			0.7	31.9	2.2	23.7	2.2	3.0	4.4
C 8H-2W	60	61	73.8	2.44	6.3	0.9	1.8	28.8		1.8						3.6		1.8			5.4	16.2	3.6	9.0	9.0	0.9	19.8
C 8H-2W	120	121	74.4	2.47		2.9		31.4			2.9					5.7		2.9			14.3	17.1		2.9	2.9	2.9	11.4
C 8H-3W	30	31	75.0	2.49			16.0	32.0							4.0	4.0		4.0			20.0	4.0	4.0	4.0	4.0	4.0	8.0
C 8H-3W	90	91	75.6	2.54	8.1	3.6		26.1		2.7	5.4			0.9		1.8		0.9			17.1	10.8	1.8	2.7	0.9		16.2
C 8H-4W	0	1	76.2	2.58	5.4	4.1		8.1								1.4					12.2	31.1	2.7	25.7	2.7		5.4
C 8H-4W	60	61	76.8	2.63	8.6	1.0		12.4			1.9							2.9			13.3	20.0	8.6	9.5	6.7	1.9	8.6
C 8H-4W	120	121	77.4	2.67	9.1			9.1								9.1		9.1			9.1	18.2		9.1			27.3
C 8H-5W	30	31	78.0	2.72	16.0			32.0							2.0	8.0		4.0			6.0	10.0		4.0			2.0
C 8H-5W	90	91	78.6	2.76	14.3			17.1										5.7			11.4	25.7	2.9	11.4			11.4
C 8H-6W	0	1	79.2	2.80	9.8	1.6	1.6	36.1							1.6	1.6					4.9	11.5	6.6	3.3			1.6
C 9H-3W	90	91	84.8	3.11	4.4	6.3		13.8	0.6	1.3	0.6		0.6		1.3			3.1		0.6	3.1	23.8	10.0	18.1	5.6		3.8
C 9H-4W	0	1	85.4	3.14	9.1	3.0	3.0	27.3								6.1					3.0	9.1	3.0	21.2			9.1
C 9H-4W	60	61	86.0	3.18	16.7	5.6		5.6								16.7					27.8	5.6		11.1			
C 9H-4W	120	121	86.6	3.21	6.4	3.7		15.6	1.8	1.8	2.8			1.8							7.3	19.3	8.3	9.2	5.5	2.8	7.3
C 9H-5W	30	31	87.2	3.24	10.0	6.0		18.0	1.0	1.0	2.0		1.0	1.0		3.0		6.0		4.0	3.0	18.0	1.0	11.0	1.0	3.0	5.0
C 9H-5W	90	91	87.8	3.28	7.5	1.9	1.3	12.6		0.6	0.6		0.6	1.3		1.9		3.8		2.5	2.5	11.9	25.2	5.7	11.9	4.4	3.1
C 9H-6W	0	1	88.4	3.31	7.8	3.5		16.5										3.5		3.5	3.5	4.3	25.2	7.8	15.7	4.3	1.7
C 9H-6W	60	61	89.0	3.34	12.5	4.5		29.5		1.1	1.1			1.1		1.1		13.6		1.1	8.0	11.4		3.4			10.2